

## **Supplementary Materials**

### **Regulating solution epitaxy of PbTiO<sub>3</sub> film by Ni ions for enhanced visible-light photovoltaic current**

**Yiran Sun<sup>1</sup>, Ruian Zhang<sup>1</sup>, Jialu Chen<sup>1</sup>, Chen Lin<sup>1</sup>, Yi Fu<sup>1</sup>, He Tian<sup>1,2</sup>, Gaorong Han<sup>1</sup>, Zhaohui Ren<sup>1,3</sup>**

1 State Key Laboratory of Silicon and Advanced Semiconductor Materials, School of Materials Science and Engineering, Zhejiang University, Hangzhou, 310027, China.

2 Center of Electron Microscope, School of Materials Science and Engineering, Zhejiang University, Hangzhou, 310027, China.

3 Shanxi-Zheda Institute of Advanced Materials and Chemical Engineering, Taiyuan, 030024, China.

**Correpondence to:** Zhaohui Ren, E-mail: renzh@zju.edu.cn

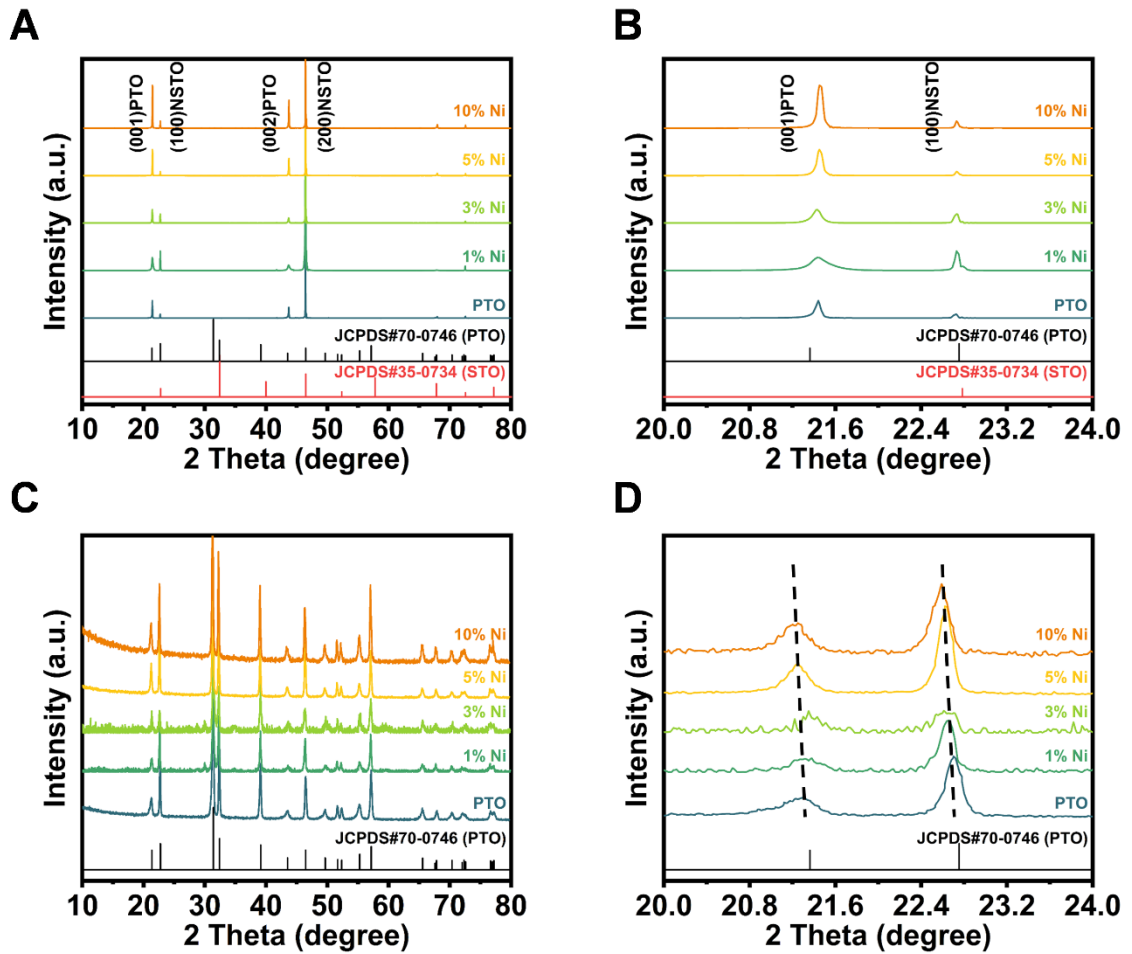


**Figure S1.** Comparative XRD analysis of films and by-product powders. (A) XRD pattern of PTO films synthesized via the coprecipitation-hydrothermal method from precursor solutions with different Ni ion concentrations of 0%, 1%, 3%, 5%, and 10%. (B) The magnification of diffraction peaks from 20.0° to 24.0° of films (001) and NSTO substrates (100). (C) XRD pattern of by-product powder synthesized from precursor solutions with different Ni ions concentrations of 0%, 1%, 3%, 5%, and 10%. (D) The magnification of diffraction peaks from 20.0° to 24.0° of powders.

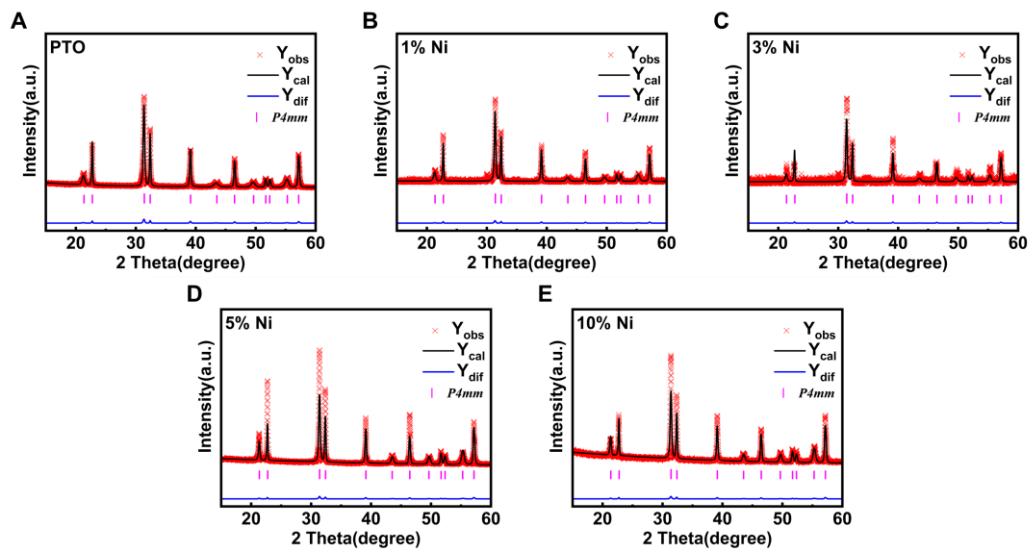


**Figure S2.** XRD pattern along with Rietveld refined data for by-product powders with different Ni ion concentrations of 0%, 1%, 3%, 5%, and 10%.

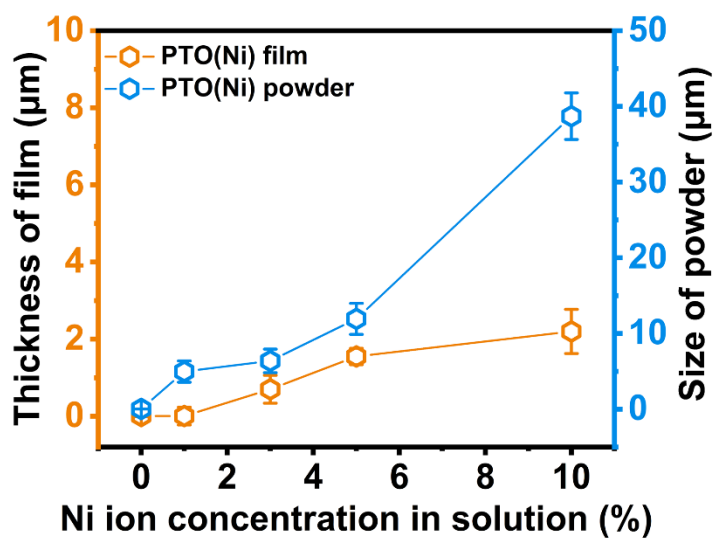


**Figure S3.** Statistics of film thickness and by-product powder size with different designed Ni ion concentrations.

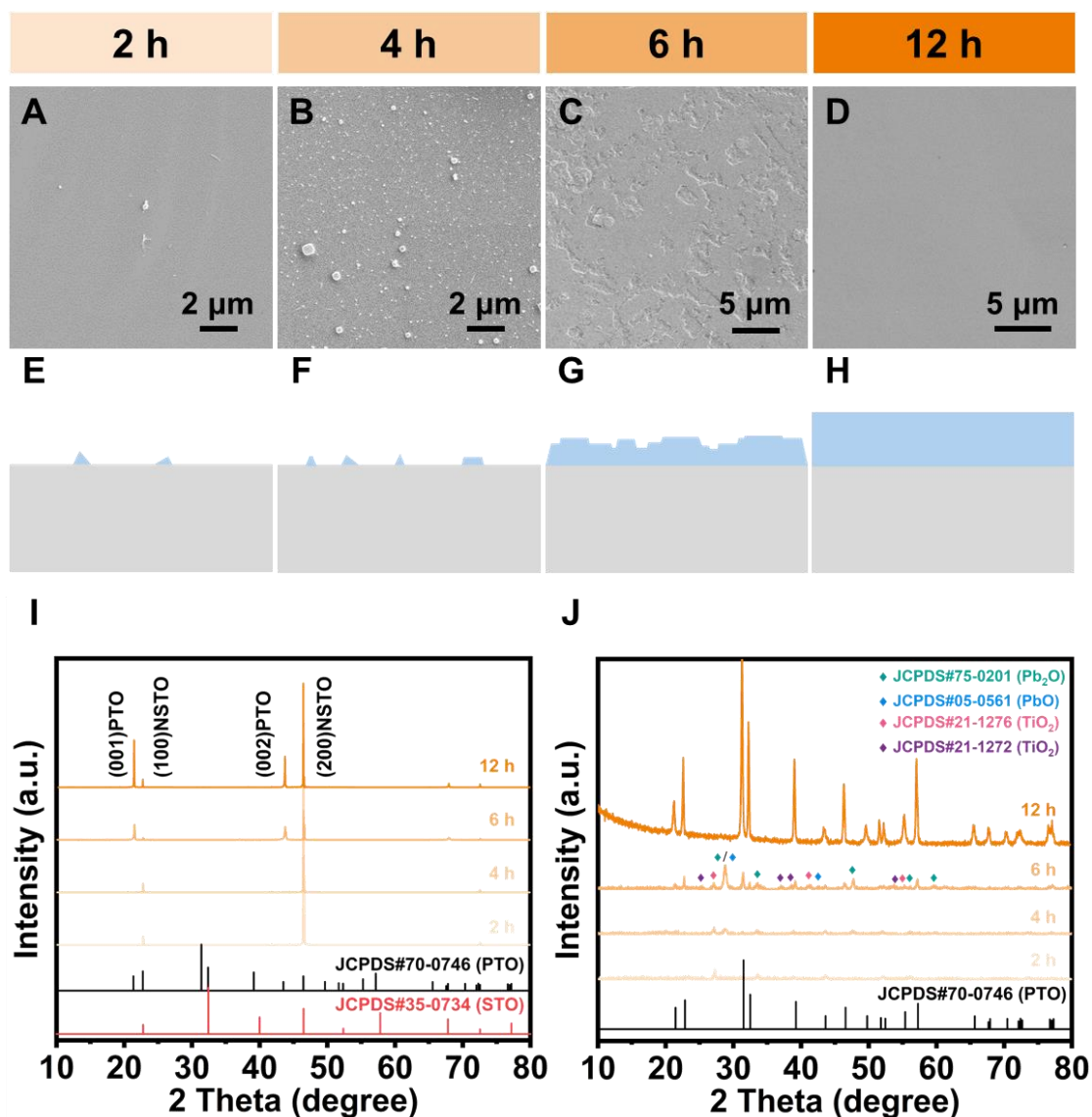


**Figure S4.** The growth process of PTO(Ni) films on NSTO substrate regulated by hydrothermal time. SEM images of PTO(Ni) films synthesized via the coprecipitation-hydrothermal method for (A) 2 h, (B) 4 h, (C) 6 h, and (D) 12 h. (E–H) The corresponding schematic diagrams of the growth models. (I) XRD pattern of PTO films synthesized with different hydrothermal times. (J) XRD pattern of PTO by-product powders synthesized with different hydrothermal times.

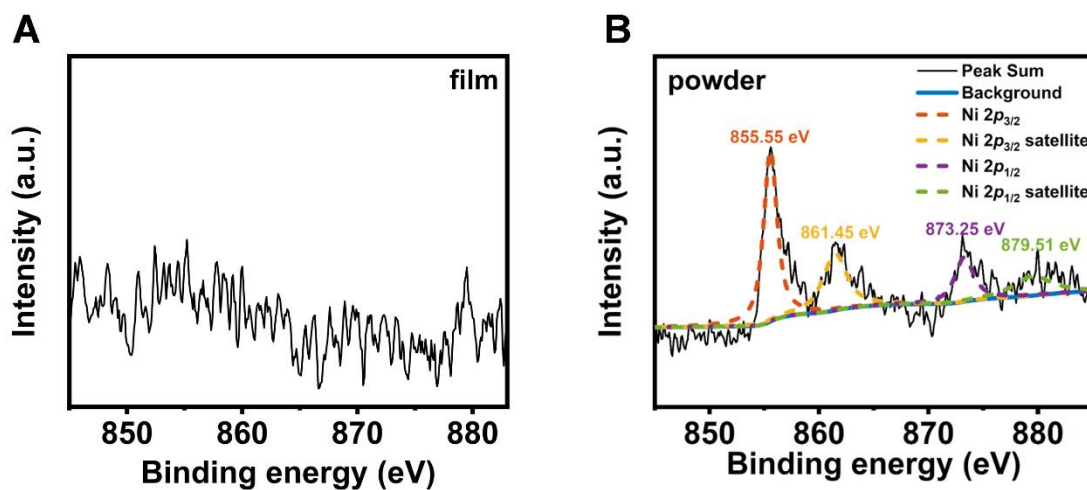


**Figure S5.** Comparative analysis of Ni content in PTO(Ni) film and by-product powder. (A) The Ni 2p XPS spectra of PTO(Ni) film. (B) The Ni 2p XPS spectra of PTO(Ni) by-product powder.

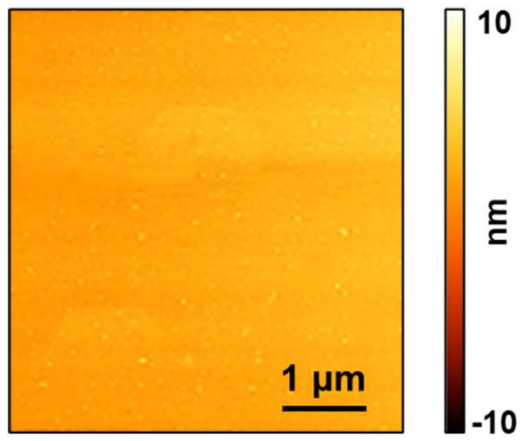


**Figure S6.** Atomic force microscopy (AFM) topography image of PTO(Ni) surface.

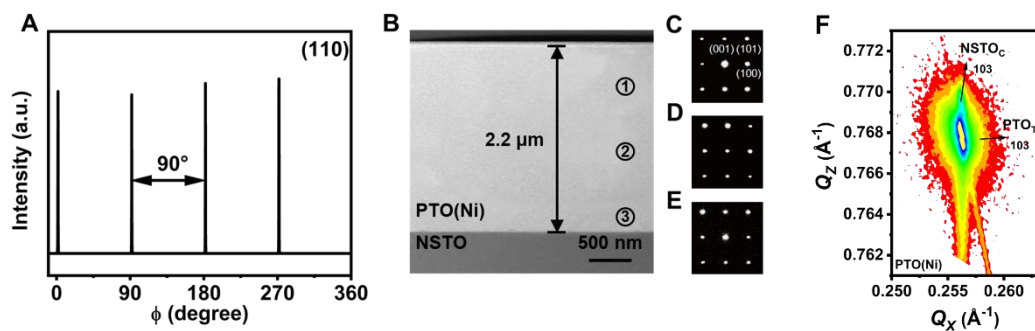


**Figure S7.** The single-crystal character of PTO(Ni) film. (A) XRD off-axis  $\phi$  scan of the (002) plane of the annealed film;  $\phi$  is the angle at which the sample rotates around its normal line. (B) Cross-section HAADF-STEM image of PTO(Ni) film. (C–E) SAED of different areas corresponding to ①, ②, and ③ in (A). (F) RSM of PTO(Ni) film.

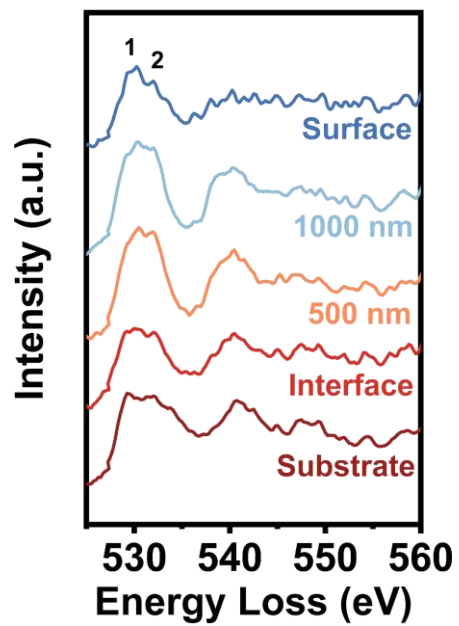


**Figure S8.** O *K* spectra perpendicular to the interface corresponding to the boxes in Figure 2B.

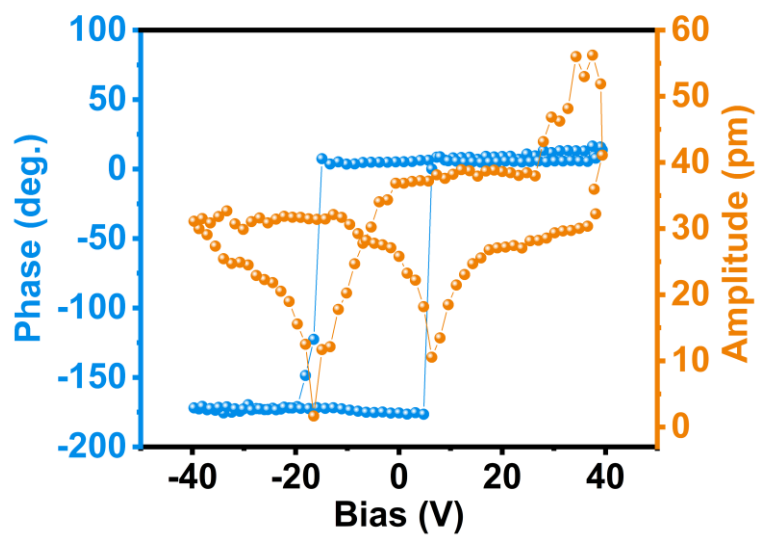


**Figure S9.** Piezoresponse amplitude curve with a “butterfly-shape” loop and piezoresponse phase curve with a hysteresis loop of PTO(Ni) film.

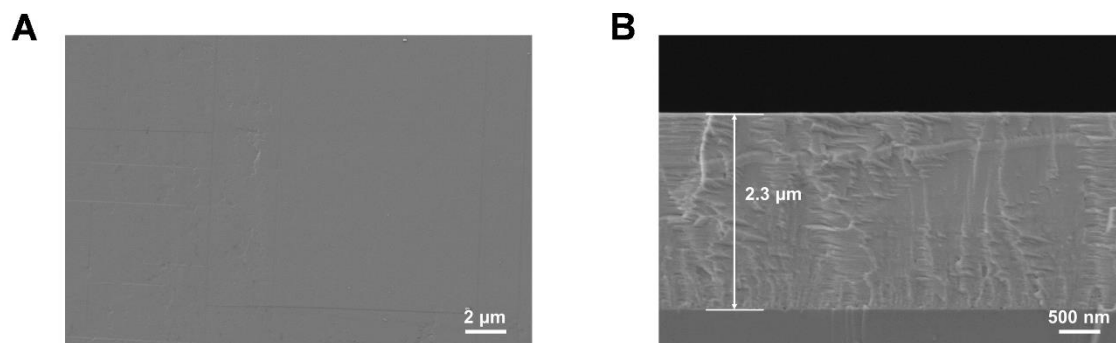


**Figure S10.** The morphology character of pure PTO film. (A) SEM image and (B) cross-sectional SEM image of pure PTO film.

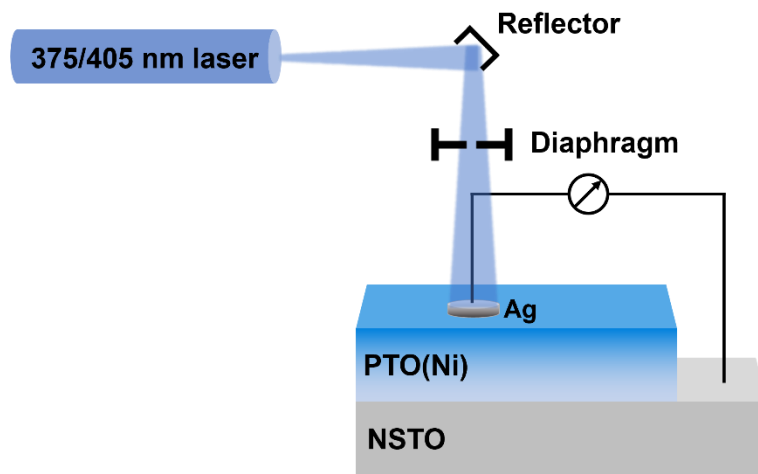


**Figure S11.** Sketch of the setup for PV measurements.

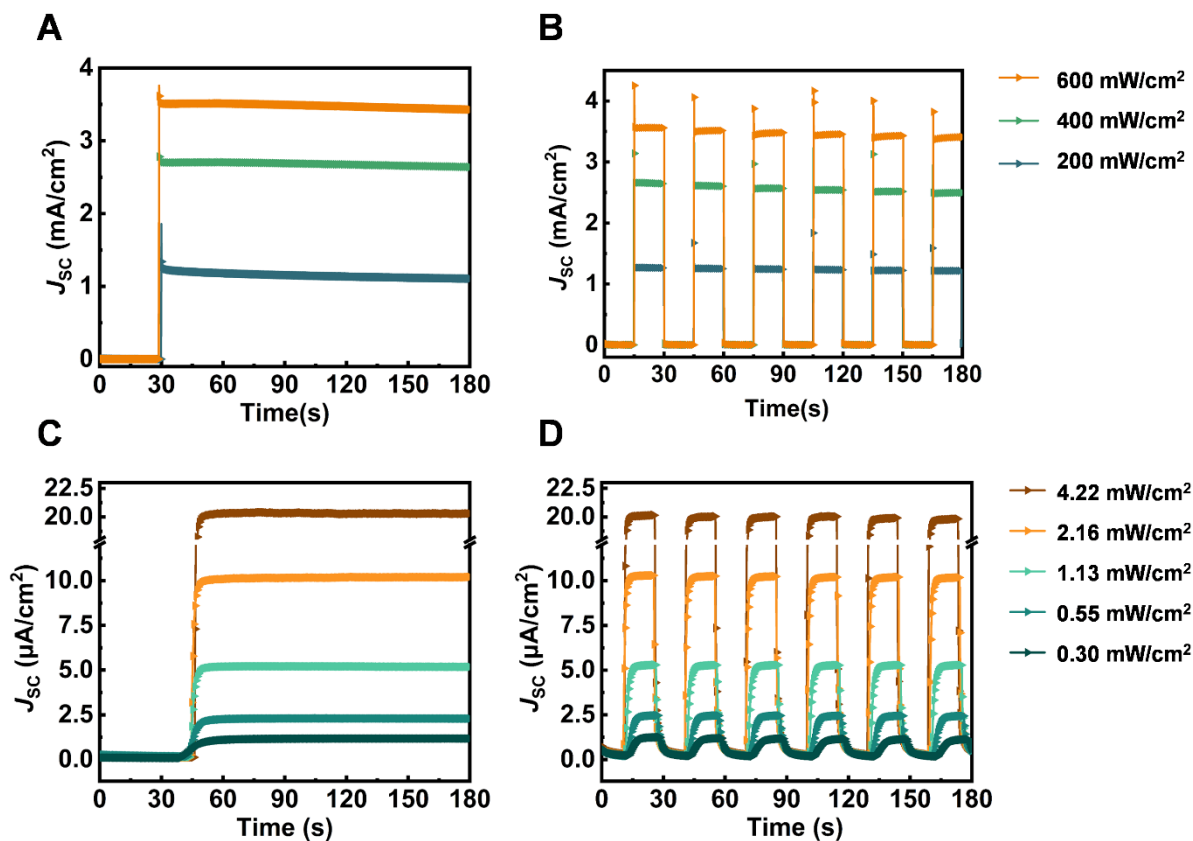


**Figure S12.** PV response of PTO(Ni) film at various light intensities. (A) Steady-state  $J_{sc}$  and (B)  $J_{sc}$  response under repeated light on and off switching of PTO(Ni) film under the irradiation of 200, 400, and 600 mW/cm<sup>2</sup>  $I_{light}$  from a 405 nm laser. (C) Steady-state  $J_{sc}$  and (D)  $J_{sc}$  response under repeated light on and off switching of PTO(Ni) film under the irradiation of 0.30, 0.55, 1.13, 2.16, and 4.22 mW/cm<sup>2</sup>  $I_{light}$  from a 405 nm laser.

**Table S1.**

Refined structural parameters and agreement factor of by-product powders with different Ni ion concentrations of 0%, 1%, 3%, 5%, and 10%.

| <b>Ni ion concentration (%)</b>             | <b>0</b>      | <b>1</b>      | <b>3</b>      | <b>5</b>      | <b>10</b>     |
|---|---------------|---------------|---------------|---------------|---------------|
| <b>Lattice parameter <math>a</math> (Å)</b> | <b>3.904</b>  | <b>3.906</b>  | <b>3.907</b>  | <b>3.907</b>  | <b>3.907</b>  |
| <b>Lattice parameter <math>c</math> (Å)</b> | <b>4.168</b>  | <b>4.161</b>  | <b>4.155</b>  | <b>4.152</b>  | <b>4.151</b>  |
| <b>Volume (Å<sup>3</sup>)</b>               | <b>63.516</b> | <b>63.490</b> | <b>63.414</b> | <b>63.393</b> | <b>63.392</b> |
| <b><math>R_{wp}</math></b>                  | <b>9.37</b>   | <b>11.21</b>  | <b>10.02</b>  | <b>10.45</b>  | <b>10.76</b>  |

**Table S2.**

EDS results of by-product powders with different Ni ion concentrations of 0%, 1%, 3%, 5%, and 10%. The Ni/Ti ratio only considers the powders without films.

| <b>Ni ion concentration<br/>(at.%)</b> | <b>0</b>     | <b>1</b>     | <b>3</b>     | <b>5</b>     | <b>10</b>    |
|--|--------------|--------------|--------------|--------------|--------------|
| <b>Pb (at.%)</b>                       | <b>17.43</b> | <b>17.26</b> | <b>17.21</b> | <b>16.75</b> | <b>16.69</b> |
| <b>Ti (at.%)</b>                       | <b>20.89</b> | <b>20.52</b> | <b>19.91</b> | <b>19.43</b> | <b>18.84</b> |
| <b>Ni (at.%)</b>                       | <b>0.00</b>  | <b>0.71</b>  | <b>0.81</b>  | <b>1.12</b>  | <b>1.97</b>  |
| <b>O (at.%)</b>                        | <b>61.68</b> | <b>61.51</b> | <b>62.07</b> | <b>62.70</b> | <b>62.50</b> |
| <b>Ni/Ti (%)</b>                       | <b>0.00</b>  | <b>1.04</b>  | <b>3.12</b>  | <b>5.36</b>  | <b>10.46</b> |

**Table S3.**

Summary of the reported photovoltaic properties in ferroelectric materials under blue light.

| <b>Materials (type) –<br/>Publication year</b>  | <b><math>J_{sc}</math> /<br/><math>\mu\text{A}/\text{cm}^2</math></b> | <b><math>V_{oc}</math><br/>/ V</b> | <b>Light<br/>wavelength / nm</b> | <b><math>I_{light}</math> /<br/><math>\text{mW}/\text{cm}^2</math></b> | <b>Photoresponsivity (<math>J_{sc}</math><br/>/<math>I_{light}</math>) / <math>\text{mA}/\text{W}</math></b> | <b>Ref.</b> |
|---|---|------------------------------------|----------------------------------|--|--|-------------|
| <b>PTO(Ni) (Epitaxial<br/>single crystal film) -<br/>this work</b>  | <b>3639.<br/>5</b>  | <b>1.0<br/>5</b>                   | <b>405</b>                       | <b>600</b>   | <b>6.066</b>   | <b>/</b>    |
| <b>PTO (Epitaxial single<br/>crystal film) - this work</b>  | <b>1019.<br/>6</b>  | <b>0.9<br/>6</b>                   | <b>405</b>                       | <b>600</b>   | <b>1.699</b>   | <b>/</b>    |
| <b>(MV)[SbI<sub>5</sub>] (MV<sup>2+</sup> =<br/>N,N-dimethyl-4,4-<br/>bipyridinium or<br/>methylviologen) (Single<br/>crystal) - 2024</b>   | <b>~0.09</b>  | <b>~5</b>                          | <b>445</b>                       | <b>168</b>   | <b><math>5.4 \times 10^{-4}</math></b>   | <b>44</b>   |
| <b>(iso-<br/>pentylammonium)<sub>2</sub>-<br/>(ethylammonium)<sub>2</sub>Pb<sub>3</sub>I<br/>10 (PEPI) (Single<br/>crystal) - 2021</b>  | <b>1.5</b>  | <b>0.7<br/>5</b>                   | <b>365-670</b>                   | <b>100</b>   | <b><math>1.6 \times 10^{-2}</math></b>   | <b>45</b>   |
| <b>(C<sub>4</sub>H<sub>9</sub>NH<sub>3</sub>)<sub>2</sub>(NH<sub>2</sub>CHNH<br/>2)-Pb<sub>2</sub>Br<sub>7</sub><br/>(DMABPb<sub>2</sub>Br<sub>7</sub>) (Single<br/>crystal) - 2021</b> | <b>102</b>  | <b>0.4</b>                         | <b>405</b>                       | <b>200</b>   | <b>0.51</b>  | <b>46</b>   |
| <b>(4-<br/>AMP)(MA)<sub>2</sub>Pb<sub>3</sub>Br<sub>10</sub>/M<br/>APbBr<sub>3</sub><br/>(heterostructure) - 2020</b>   | <b>0.047<br/>6</b>  | <b>0.2<br/>33</b>                  | <b>405</b>                       | <b>0.04</b>  | <b>1.19</b>  | <b>47</b>   |

|   |                          |                        |                |              |                              |           |
|---|--------------------------|------------------------|----------------|--------------|------------------------------|-----------|
| <b>(BPA)<sub>2</sub>PbBr<sub>4</sub> (BPA=3-bromopropylammonium) (Single crystal) - 2020</b>                            | <b>4.5</b>               | <b>0.8</b><br><b>5</b> | <b>377</b>     | <b>45</b>    | <b>0.1</b>                   | <b>48</b> |
| <b>BaTiO<sub>3</sub> (BTO1) (Ceramics) - 2019</b>   | <b>0.262</b>             | <b>0.1</b>             | <b>405</b>     | <b>131</b>   | <b>2×10<sup>-3</sup></b>     | <b>43</b> |
| <b>(EA)<sub>2</sub>(MA)<sub>2</sub>Pb<sub>3</sub>Br<sub>10</sub> (Single crystal) - 2019</b>                            | <b>4.1</b>               | <b>0.9</b><br><b>8</b> | <b>405</b>     | <b>100</b>   | <b>4.1×10<sup>-2</sup></b>   | <b>49</b> |
| <b>BaTiO<sub>3</sub> (BTO2) (Ceramics) - 2017</b>   | <b>0.039</b>             | <b>0.3</b>             | <b>405</b>     | <b>111.1</b> | <b>3.5×10<sup>-4</sup></b>   | <b>42</b> |
| <b>CH<sub>3</sub>NH<sub>3</sub>PbI<sub>3</sub> (MAPbI<sub>3</sub>) (Single crystal) - 2016</b>                          | <b>4</b>                 | <b>0.7</b><br><b>5</b> | <b>405</b>     | <b>1</b>     | <b>4</b>                     | <b>50</b> |
| <b>Mn- and Zn-codoped BiFeO<sub>3</sub> (BFMZO) (Epitaxial film) - 2016</b>   | <b>549.9</b><br><b>5</b> | <b>145</b>             | <b>405</b>     | <b>17000</b> | <b>~3.24×10<sup>-2</sup></b> | <b>41</b> |
| <b>0.65PbTiO<sub>3</sub>-0.35Bi(Ni<sub>2/3</sub>Nb<sub>1/3</sub>)O<sub>3-δ</sub> (0.65PT-0.35BNN) (Ceramics) - 2015</b> | <b>0.116</b>             | <b>10</b>              | <b>400–780</b> | <b>200</b>   | <b>5.8×10<sup>-4</sup></b>   | <b>14</b> |
| <b>Bi(Fe<sub>0.6</sub>Sc<sub>0.4</sub>)O<sub>3</sub> (BFSO) (Epitaxial film) - 2015</b>                                 | <b>7</b>                 | <b>0.6</b>             | <b>435</b>     | <b>22.3</b>  | <b>0.3139</b>                | <b>51</b> |
| <b>Bi<sub>0.88</sub>Ce<sub>0.12</sub>Fe<sub>0.9</sub>Mn<sub>0.1</sub>O<sub>3</sub> (BCFM) (Epitaxial film) - 2014</b>   | <b>241</b>               | <b>0.5</b>             | <b>405</b>     | <b>160</b>   | <b>1.53125</b>               | <b>52</b> |
| <b>polycrystalline BiFeO<sub>3</sub> (Poly-BFO) (Epitaxial film) - 2011</b>   | <b>1</b>                 | <b>0.1</b>             | <b>450</b>     | <b>340</b>   | <b>~2.9×10<sup>-3</sup></b>  | <b>53</b> |
| <b>BiFeO<sub>3</sub> (BFO1) (Epitaxial film) - 2010</b>   | <b>0.4</b>               | <b>0.3</b>             | <b>435</b>     | <b>0.75</b>  | <b>0.5333</b>                | <b>54</b> |

|  |             |            |                |             |                            |           |
|--|-------------|------------|----------------|-------------|----------------------------|-----------|
| <b>Pb(Zr<sub>0.2</sub>Ti<sub>0.8</sub>)O<sub>3</sub></b>   |             |            |                |             |                            |           |
| <b>(PZT20/80) (Epitaxial film) - 2009</b>                  | <b>8</b>    | <b>/</b>   | <b>350–450</b> | <b>10</b>   | <b>0.8</b>                 | <b>55</b> |
| <b>BiFeO<sub>3</sub> (BFO2)</b>                            |             | <b>0.2</b> |                |             |                            |           |
| <b>(Epitaxial film) - 2009</b>                             | <b>0.4</b>  | <b>86</b>  | <b>435</b>     | <b>750</b>  | <b>5.3×10<sup>-4</sup></b> | <b>56</b> |
| <b>Pb(Zr<sub>0.52</sub>Ti<sub>0.48</sub>)O<sub>3</sub></b> |             |            |                |             |                            |           |
| <b>(PZT52/48) (Epitaxial film) - 2000</b>                  | <b>0.03</b> | <b>0.8</b> | <b>300–390</b> | <b>0.05</b> | <b>0.6</b>                 | <b>57</b> |

---